ARTICLE

Microfluidic platform integrating Caco-2 spheroids-on-chip for real-time investigation of intestinal epithelial interaction with bacterial extracellular vesicles

Silvia Tea Calzuola[a,b*], Debora Pinamonti[c], Francesco Rizzotto[d], Jeanne Malet-Villemagne[d], Céline Henry[d], Christine Péchaux[e,f], Jean Baptiste Blondé[b], Emmanuel Roy[b], Marisa Manzano[c], Goran Lakisic[d], Sandrine Truchet[d], Jasmina Vidic[d*]

Campylobacter jejuni is the most common cause of foodborne gastroenteritis in humans with about 550 million annual infections worldwide. The extracellular vesicles (EVs) of *C. jejuni* have an important impact during pathogenicity but their role in invasion of the host intestinal epithelial cells remains largely unknown. *In vitro* models lack the complexity of tissue and fail to replicate the dynamic interactions between EVs and human intestinal epithelial cells accurately, while animal infection models bring ethical concerns. To bridge this gap, we propose a microfluidic platform integrated with an impedimetric sensor for real-time monitoring of *C. jejuni* EVs' interaction with human intestinal epithelial cells. When cultured in this microfluidic device, Caco-2 epithelial cells underwent spontaneous 3D morphogenesis and spatially organised in spheroid-like structures. Functional assays revealed that *C. jejuni* secretome and EVs have a significant cytotoxic effect on Caco-2 cultured on plates. However, 3D Caco-2 spheroids showed increased resistance to the toxicity of secreted virulence factors of *C. jejuni*. By combining impedance spectroscopy and microscopic observation, the platform allowed real-time monitoring of cellular spatial growth and sensitive detection of the Evs' ability to reach and damage intestinal epithelial cells organised in 3D morphologies. Thus, the developed microfluidic device offers a promising platform for investigating host-microbe interactions and may have a broad impact on biomedical research on gastroenteritis.

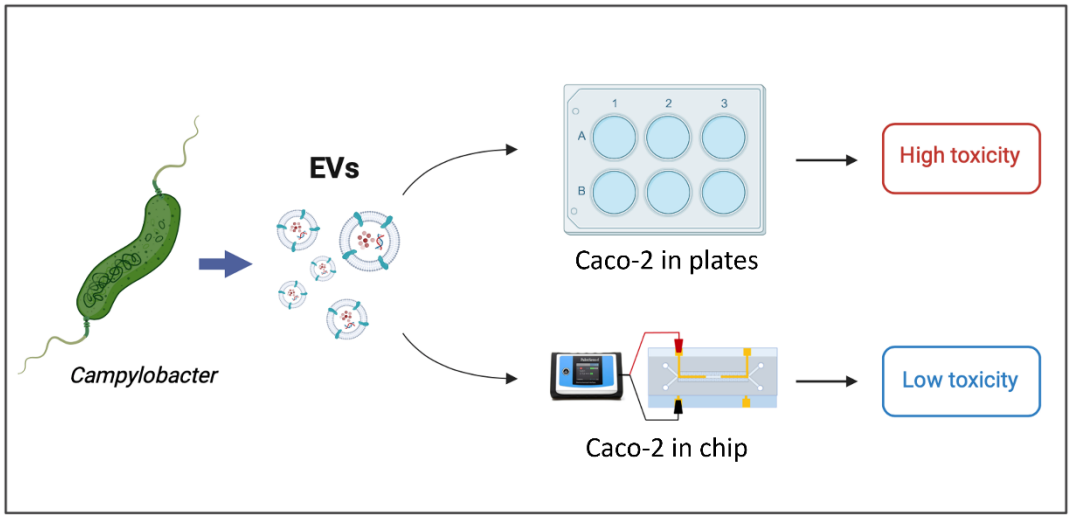

[a] UMR7646 Laboratoire d'hydrodynamique (LadHyX), Ecole Polytechnique, Palaiseau, France

[b] Eden Tech, Paris, France

[c] Department of Agriculture Food Environmental and Animal Sciences, University of Udine, 33100, Udine, Italy

[d] Micalis Institute, INRAE, AgroParisTech, Université Paris-Saclay, Jouy en Josas, France

[e] Université Paris-Saclay, INRAE, GABI, Jouy en Josas, France.

[f] MIMA2 Imaging Core Facility, Microscopie et Imagerie des Microorganismes, Animaux et Aliments, INRAE, Jouy en Josas, France.

Introduction

Infectious diseases are a major cause of disability and death in humans and are recognised as a leading cause of health loss globally[1]. *Campylobacter* is the most common zoonotic cause of diarrheal diseases worldwide. Species from the genus *Campylobacter* are Gram-negative, microaerophilic spiral-shaped polar rods, whose characteristic corkscrew-like motility is mediated by an unsheathed flagellum at one or both ends. The most frequently reported *Campylobacters* in human

diseases are *Campylobacter jejuni* and *Campylobacter coli*, and over 80% of *Campylobacter*iosis is due to *C. jejuni*[2]. The main source of *Campylobacter*iosis is contaminated undercooked poultry meat, followed by unpasteurised milk, unwashed vegetables, and water. Contamination of meat occurs mainly from faecal content to the meat during the slaughtering process because *Campylobacter* colonises the gastrointestinal tract of birds and warm-blooded mammals (such as pigs and sheep) without causing any symptoms[3]. In contrast, the ingestion of only 500 cells of *C. jejuni* is sufficient to trigger disease in humans[4]. The clinical symptoms of human *Campylobacter*iosis include diarrhoea (frequently bloody), abdominal pain, fever, headache, nausea, and vomiting, which can last up to two weeks. Severe complications occur in about 1% of cases, such as Guillain-Barré syndrome, inflammatory bowel disease, and arthritis[5].

Despite *C. jejuni* being one of the most common foodborne pathogens worldwide, the mechanisms of its pathogenesis and host colonisation have not yet been fully clarified, primarily due to difficulties in establishing relevant animal models. *In vivo* tests are expensive, labour-intensive, time-consuming, and often fail to predict accurately clinical responses during *C. jejuni* infection in humans[6,7]. Alternatively, *In vitro* host-microbe co-cultures provide practical platforms for investigating specific questions. The investigation of *Campylobacter* infection in conventional cell culture models, such as plates and Transwell, has suggested that several virulent factors are involved in bacterial-host interactions[8–12]. The impact of *C. jejuni* extracellular vesicles (EVs) and their proteic cargo on epithelial cells has been of particular interest[13–15] because the bacterium relies on this alternative secretion pathway to secrete biomolecules[7]. However, 2D platforms cannot allow dynamic studies and are ineffective in explaining how bacterial cells or their vesicles cross the epithelial barrier to invade the host. Recent studies have shown that forces such as shear stress and mechanical strain in the context of host-microbe interaction appear to play a crucial role in bacterial pathogenicity[16–19], but their effects are difficult to assess using conventional 2D *In vitro* models. Therefore, there is a strong interest in developing alternative experimental 3D platforms to mimic key aspects of human gut epithelium for studying *C. jejuni* diseases.

Organs-on-a-chip are microfluidic cell culture devices designed to accurately replicate organ-level physiology by reconstructing tissue-tissue interfaces, mechanical signals, fluid flow, and the biochemical cellular microenvironment[20]. Microfluidic technologies offer a distinct advantage in bridging the gap between *In vitro* experimental models and *In vivo* pathophysiology. For instance, it has been shown that the topology and peristaltic cycles simulated by guts-on-chip are essential to reproduce the virulent outcome of *Shigella flexneri* infections reported in clinical studies[21], as well as the dynamics of infection of *Entamoeba histolytica*[22]. Through a similar organ-on-chip model, Kim et al.[23] exposed intestinal epithelial cells to physiological levels of fluid shear stresses and cyclic strains showing that peristaltic deformations are the main responsible for preventing uncontrolled growth of commensal bacteria in the gut, in accordance with clinical observations[24].

Here we present a new microfluidic platform with integrated microelectrodes that allows investigation of *Campylobacter* EVs interaction with human intestinal epithelial cells. To achieve this, we designed a two-channel, user-friendly microfluidic system. When Caco-2 cells were cultured on one side of the porous membrane, they underwent spontaneous 3D morphogenesis. We evaluated the cytotoxicity of EVs secreted by *C. jejuni* on Caco-2 cells in 2D *In vitro* models and within the microfluidic device and demonstrated the crucial role of the spatial organisation of epithelial cells on the effect of bacterial EVs-secreted virulence factors.

Materials and methods

Materials and reagents

Flexdym™ was supplied by Eden Tech (France). Poly(methyl methacrylate) (PMMA) was purchased from Oracal Polikarbonati (Serbia). Polyester membranes were supplied by GVS Corporation (Italy). Columbia agar and brain-heart-infusion (BHI) broth or agar, horse defibrinated blood, cell culture medium Dulbecco's Modified Eagle Medium (DMEM), foetal calf serum (FCS), L-glutamine (GlutaMax), Phosphate Buffer Solution (PBS), and Trypsin 2.5% were purchased from Gibco via Thermo Fisher Scientific (France). Matrigel Basement Membrane Matrix were purchased from BD Scientific (France). Hoechst blue 33342, Propidium Iodide, and Alexa Fluor 488-conjugated Wheat Germ Agglutinin (WGA-AF488) were purchased from Thermo Fisher Scientific (France). Odixanol, uranyl acetate, glutaraldehyde, dimethyl sulfoxide (DMSO), 3-(4,5-dimethylthiazol-2-yl)-2,5-diphenyltetrazolium bromide (MTT), ammonium bicarbonate, iodoacetamide, dithiolthreitol (DTT), and hydrogen peroxide (H_2O_2) were purchased from Sigma (France).

Cell line, *Campylobacter* strain, and culturing

Human colorectal carcinoma cell line (Caco-2, ATCC HTB-37) were routinely cultured in DMEM containing GlutaMax, 100 IU/ml of penicillin, 100 µg/ml of streptomycin and 20% FCS at 37°C in a humidified 10 % CO_2 atmosphere following the ATCC recommendations. Cells were routinely maintained in T25 flasks and passaged twice per week.

The atypical aerotolerant strain *Campylobacter jejuni* strain Bf[25] was cultured on Columbia agar medium supplemented with horse blood (5%) at 42°C under microaerophilic conditions using the candle jar for 16h. Overnight cultures in BHI supplemented with horse blood (0.4%) were used to recover supernatant for EVs purification.

Purification and size characterisation of EVs

C. jejuni cells grown in BHI supplemented with horse blood until saturation phase (10 mL) were removed by filtration through a 0.20 µm membrane filter (Whatman, GE Healthcare Life Science). The supernatant was ultra-centrifuged at 120,000 x g for 2 h in an SW41 rotor using a Beckman XL-90 ultracentrifuge to pellet down the EVs. The resulting vesicle pellet was suspended in PBS, and then added on a three-layer iodixanol

discontinuous gradient of 45%, 26% and 10% (w/v) in SM buffer (50 mM Tris pH7.5, 100 mM NaCl, 10 mM $MgCl_2$). Tubes were ultra-centrifuged at 200,000 x g for 5h in an SW55 rotor. The resulting fractions containing EVs were pooled (1.8 ml). The aliquots were used immediately or stored at 4°C and used within a week.

The total protein concentration of purified secretome and EVs was determined by Bradford assay (Biorad, France). The EV hydrodynamic diameter was determined by dynamic light scattering (DLS) using the Zetasizer Pro (Malvern, France). The scattering intensity data were processed using the instrumental software to obtain the size distribution of particles. A total of 15 scans with an overall duration of 5 min were performed for each sample. Measurements were done at 20°C. To determine the number of released vesicles and their sizes, samples were characterised by nano-flow cytometry (nFCM) using a NanoAnalyser (NanoFCM Co., Ltd, Nottingham, UK) according to manufacturer instructions. The MemGlow staining was performed to observe the purity of the EV samples by measuring the fluorescence positivity in one channel (green = 525/40 bandpass filter). Particle concentration and size distribution were calculated using nFCM software (NF Profession V1.08).

Electron microscopy

To visualise vesicle release from *C. jejuni*, bacterial cells in saturation phase were fixed with 2% glutaraldehyde in 0.1 M sodium cacodylate buffer (pH 7.2) at room temperature for 1 h and gradually dehydrated as described previously[26]. Samples were then substituted gradually in a mixture of propylene oxide epon and embedded in Epon (Delta Microscopy, Labège, France). Thin sections (70 nm) of bacterial preparation were collected onto formvar/carbon-coated 200-mesh copper grids (Agar Scientific) and counterstained with lead citrate to allow transmission electron microscopy (TEM) visualisation. Purified vesicles were directly adsorbed onto copper grids. After deposition of the samples, grids were washed twice for 1 min with PBS, and negatively stained by floating on a 10-µl drop of 2% (w/v) uranyl acetate for 1 min. The grids were air-dried before observation under a Philips EM12 electron microscope at 80 kV exciting voltage. Images were acquired with a charge-coupled device camera (AMT).

In addition, *C. jejuni* cells after fixation were mounted on aluminium stubs (50 mm diameter) with carbon adhesive discs (Agar Scientific, Oxford Instruments SAS, Gomez-la-Ville, France) and visualised by field emission gun scanning electron microscopy (SEM) under high vacuum conditions with a Hitachi SU5000 instrument (Milexia, Verrières-le-Buisson, France). Electron Microscopy analyses were performed at the Microscopy and Imaging Platform MIMA2 (INRAE, Jouy-en-Josas, France).

Proteome analysis

Proteomic analysis was performed on *C. jejuni* secretome containing EVs. Proteins were resuspended in Laemmli buffer and loaded on SDS-PAGE (short migration). Bands of gel were cut and proteins were reduced with DTT (10 mM) for 30 minutes at 56°C and alkylated with iodoacetamide (final concentration 55 mM) for 45 min at room temperature in the dark. In-gel digestion was conducted with 50 mM ammonium bicarbonate pH 8.0 overnight at 37°C with 300 ng trypsin (Promega) per sample. Peptides were extracted by 5% formic acid in water/acetonitrile (v/v). Supernatant and extracted tryptic peptides were dried and resuspended in 100 µL of 0.1% (v/v) formic acid and 2% (v/v) acetonitrile.

Mass spectrometry was performed by coupling an Orbitrap Fusion™ Lumos ™ Tribrid ™ (Thermo Fisher Scientific) with an UltiMate™ 3000 RSLCnano System (Thermo Fisher Scientific) at the PAPPSO platform, Jouy en Josas, as explained before[26]. 4 µl were injected and range mass m/z: 400-1500, analysed charge states were set to 2–5, the dynamic exclusion to 60 s and the intensity threshold was fixed at 1 × 104, and (ii) MS/MS using HCD (30% collision energy) in Orbitrap (AGC target = 5.0 × 103 max. injection time = 100 ms).

Data analysis was performed using the *C. jejuni* Bf subsp jejuni NCTC 11168 (ATCC 700819) database (NCBI, version 2021, 1572 entries) and the X!TandemPipeline (open source software developed by PAPPSO, version 0.4.5). Protein identification was run with a precursor and a fragment mass tolerance of 10 ppm. Enzymatic cleavage rules were set to trypsin digestion ("after Arg and Lys, unless Pro follows directly after") and no semi-enzymatic cleavage rule was allowed. The fix modification was set to cysteine carbamidomethylation and the potential modification was set to methionine oxidation. The peptide E-value < 0.01 with a minimum of 2 peptides per protein and protein E-value of <10−4 were used as criteria to filter identified proteins.

DNA analysis

The NanoFCM equipped with two channels (green = 525/40 bandpass filter, red = 670/30 bandpass filter) was used to estimate DNA distribution in EVs of different sizes. Freshly filtered (0.2 µm) PBS was analysed as background signal and subtracted from the sample measurements. The LIVE/DEAD BacLight kit (Thermo Fisher Scientific, France) was used to label DNA within or attached to vesicles. Stained EVs were diluted with PBS, resulting in particle counts in the optimal range of 2,500-12,000 events.

Infection assay on plates: MTT test

The MTT test was performed to determine the toxicity of *C. jejuni* secretome or EVs on Caco-2 cells. Caco-2 cells were plated at a density of 30,000 cells per well on 96-well plates. After 48 h, cells were incubated with EVs at MOI of 10 (according to vesicle enumeration using nano-flow cytometry) or supernatant at 0.08 mg/mL total protein and incubated for 24 h. Then, a freshly prepared MTT at a final concentration of 0.8 mg/ml was added and incubated at room temperature for 1 h. Subsequently, the cell layer was dried and MTT formazan produced by conversion of the water-soluble MTT was solubilised in DMSO as previously described[27]. Cell survival was quantified by measuring absorbance values assessed at 560 nm and corrected for a

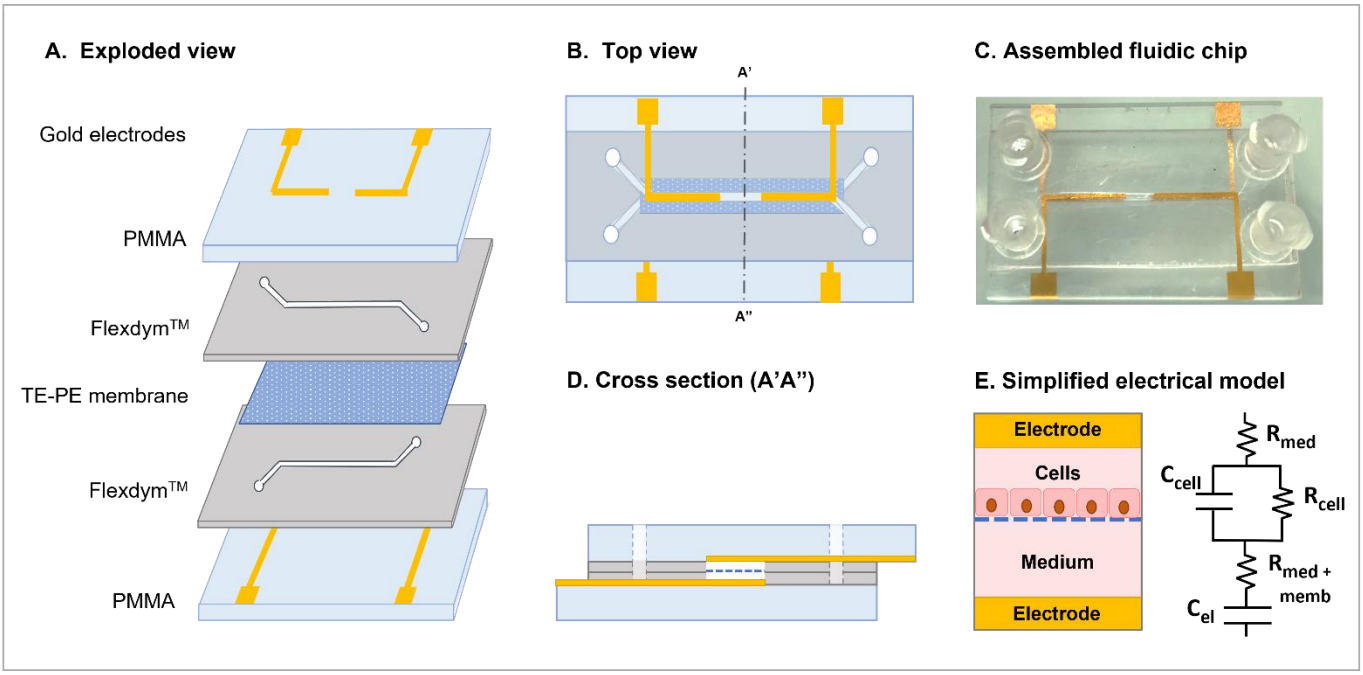

Figure 1: Multilayer chip design with integrated membrane and electrodes. A) Exploded view showing the materials of the microfluidic device: clear PMMA with 3D printed gold electrodes, Flexdym, and polyester track-etched membrane **B)** Top view of the chip. **C)** Cross-section showing the apical and basal microchannels. The microchannels are 2 cm long, 1 mm wide, 250 µm high. **D)** Photograph of the assembled organ chip (with connectors). **E)** Simplified electrical model.

background signal by subtracting the signal measured at 670 nm using Tecan Spark®. Cell survival was expressed as % of cells treated only with PBS (20%).

Chip design and fabrication

The gut-on-chip with integrated electrodes is composed of five layers: two electrode layers, two microfluidic channels, and a porous membrane dividing the apical from the basal section of the gut-on-chip (**Figure 1**).

The geometry of channels and electrodes was designed using CAD software (Autodesk Inventor). The outer layers were comprised of 2 mm thick PMMA slides that were the substrate for the 50 nm-thick gold electrodes. Two "L-shaped" electrodes (L:2.25cm; W:1mm) were printed on each PMMA slide. Four circular through-holes were then drilled on the PMMA upper layer, serving as inlets and outlets for the apical and basal channels. A plot cutter was used to cut out the channels' design (L:2.5cm; W:1mm) from the 250 µm-thick Flexdym sheets, forming the two middle fluidic layers. A polyester track-etched membrane with pore size of 5 µm, and pore density of $4 \cdot 10^5$ pores/cm^2 separated the apical and basal fluidic channels and served as the substrate for cell culture. The five layers are aligned and assembled layer-by-layer, then the assembled device is placed at 100°C under moderate weight for 1 hour to ensure a leak-free bonding. We exploited the unique bonding properties of Flexdym to seamlessly bond all layers of the chip without adhesives or surface treatments. We produced, aligned and bound several chips in less than 2 hours. For microscopy investigation, a gut-on-chip without electrodes is fabricated by hot embossing.

An aluminium mould with the channel design (L:2.5cm; W:1mm; H:250 µm) was produced by CNC machining and used to fabricate 750 µm-thick Flexdym chips by hot embossing (3 minutes, 150°C, 0,7 bar) with the Sublym machine (Eden Tech). The same polyester track-etched membrane was used to separate the apical and basal channels. The three layers were aligned, assembled, and bonded at 100°C for 1 hour under moderate weight.

Infection assay

Caco-2 cells were used as a model of the intestinal epithelial cells. Before cell seeding, the microfluidic channels and connectors were sterilised with 70% ethanol. Once ethanol was fully evaporated, the devices were rinsed with sterile PBS. For microfluidic cell culture, Caco-2 cells were suspended at a concentration of $3 \cdot 10^6$ cells/mL in a Matrigel solution at a ratio of 1:3 with the culture medium. 200 µl of cell suspension were then loaded into the apical channel. After seeding, cells were cultured statically changing the medium once per day. DMEM with 10% FCS, 1% L-glutamine, and 3% Penicillin-Streptomycin was used for the microfluidic culture. Epithelial cells inside the chip were infected after 48 hours of culturing using *C. jejuni* secretome (0.08 mg/mL total protein), purified EVs (MOI 10), and PBS (20%) as negative control for 24h. Positive control was 1 mM H_2O_2 which killed all cells.

Impedance Spectroscopy

Impedance spectra were acquired with a PalmSens4 potentiostat/galvanostat (PalmSens BV). An alternating current

with a 0.1 V amplitude was applied between an apical and basal electrode across a frequency range from 10 kHz to 100 kHz, resulting in 53 impedance measurements. Each frequency scan required approximately 2 minutes and the measure was repeated three times. Before each measurement, cells were gently rinsed, and the apical and basal channels were filled with fresh culture medium to ensure consistency in the medium composition with respect to the baseline.

Image acquisition and analysis

Images were acquired with an Axio-Observer Z1 inverted fluorescence microscope (Zeiss) equipped with an AxioCam MRm digital camera and fluorescence filters, using a x10/0.25 P A-Plan objective or a x20/0.8 Apochromat objective (all Zeiss). Microfluidic chips were imaged 4 hours after seeding to check the starting cell confluency in each device. The Caco-2 were also imaged on day 2 before infection, on day 3 i.e., 24h post-infection (p.i.). Live cells' nuclei were stained with Hoechst blue 33342 (1:100), dead cells were stained with Propidium Iodide (PI, 2µM), and cell membranes were stained with WGA-AF488 (1:500). The culture medium used in microfluidic experiments was supplemented with 25 mM HEPES before live imaging to improve the buffering capacity of DMEM and reduce cell stress during image acquisitions. Acquired images were processed using ZEN Lite 3.9 image acquisition software (Zeiss).

Results and Discussion

Campylobacter extracellular vesicles (EVs)

Like other bacteria, *C. jejuni* releases EVs during all growing phases that contribute to its function and interaction with the host[7,14,28]. Ultrathin sections of *C. jejuni* cells at stationary phase examined by transmission electron microscopy (TEM) revealed vesicle-like structures protruding from bacterial cells (**Figure 2A**). Scanning electron microscopy (SEM) also revealed the presence of small spherical structures surrounding the bacterial cells or attached to bacterial cells (**Figure 2B**). We isolated the EVs by collecting and filtering the culture broth to remove the extracellular medium from bacterial cells. Crude EVs were pelleted by ultracentrifugation from the extracellular medium and then purified by density gradient ultracentrifugation (**Figure 2C**).

All fractions were visualised by negative staining TEM and those containing EVs were pooled and dialysed against this buffer to remove iodixanol. As shown in **Figure 2D**, the purified EVs were of typical round shape with diameters ranging from 20 to 200 nm. Additionally, we explored the hydrodynamic diameter (R_H) of EVs by performing DLS measurements. Before EVs purification, *C. jejuni* secretome showed a population of particles having R_H between 10 and 30 nm, that probably corresponded to secreted proteins and their aggregates, and a population having the mean R_H of 212 nm that corresponded to expected diameters of EVs (**Figure 2E**). After the gradient density purification step, only the 212 nm diameter population was detected, strongly suggesting that vesicles were purified from biomolecules in external medium. Nevertheless, the sizes determined from DLS measurements are overestimated because vesicles in solution are dynamic and solvated.

Therefore, we estimated the purity, size and amount of EVs by the nano-flow cytometry after staining the putative EVs with MemGlow membrane dye. As shown in **Figure 2F**, EVs ranged in size from 50 to 100 nm, with a median size of ~70 nm. The purity of EVs was 95%. Following the protocol in **Figure 2C**, the concentration of the purified EVs ranged from $1{\cdot}10^8$ to $6{\cdot}10^8$ vesicles/ml. Thereafter, the Syto9/Propidium Iodide (PI) assay, commonly used to distinguish live/dead bacteria, was used to stain nucleic acids in the EVs. As PI is not membrane permeable in contrast to Syto9, it was possible to detect external and internal DNA. Interestingly, DNA was mostly present in EVs having diameters close to the median size while smaller contained no nucleic acid (**Figure 2G**). Extracellular DNA is involved horizontal gene transfer, supply of nutrients and biofilm formation in *Campylobacter*[29,30]. However, extracellular DNA is a versatile molecule that may impact the innate and cell-mediate immune response of host-cells[31,32].

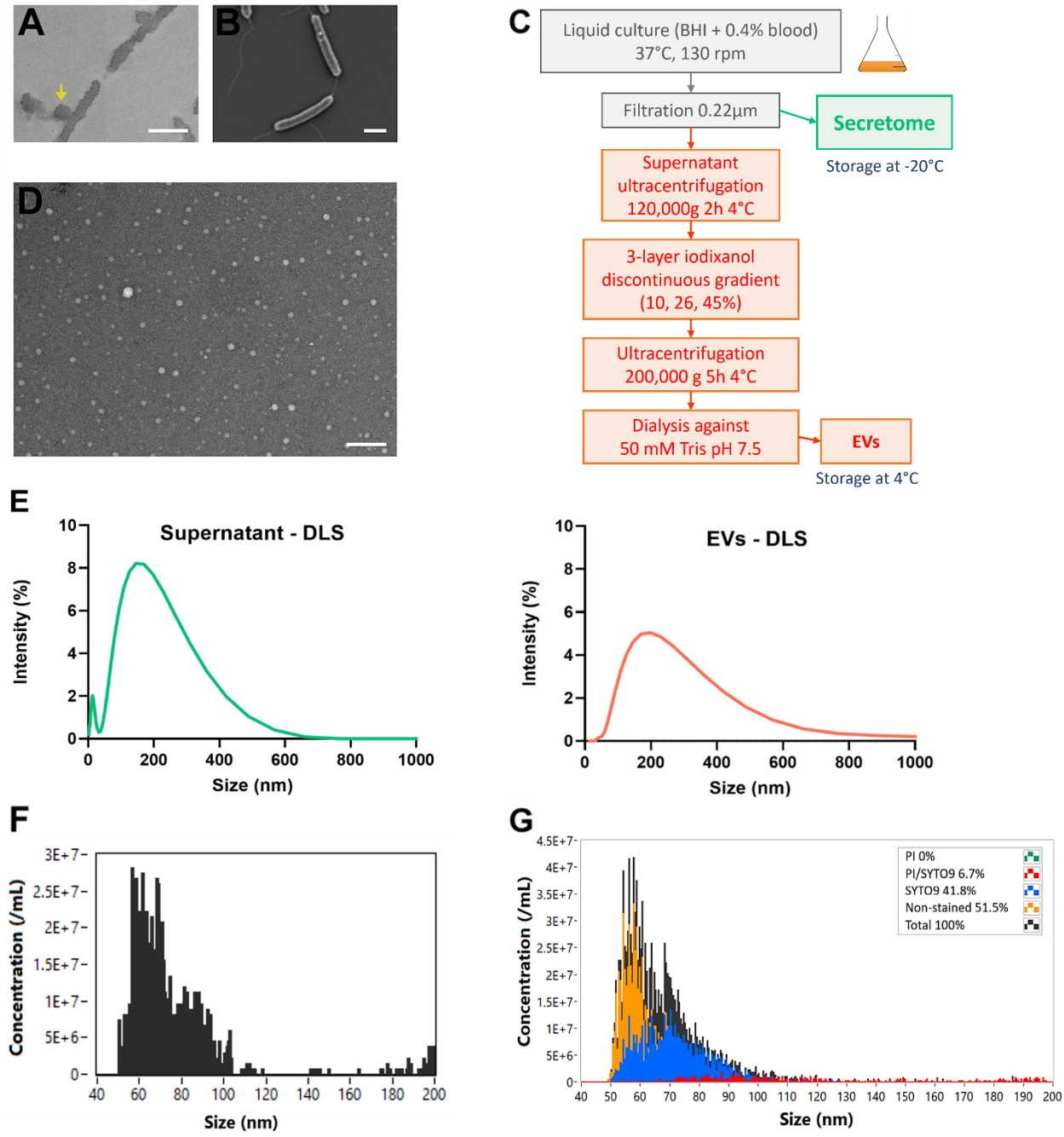

Figure 2: Characterisation of *C. jejuni* secretome and extracellular vesicles (EVs). A) Transmission electron microscopy (TEM) image of *C. jejuni* at stationary phase with vesicle-like structures indicated by the arrow. **B)** Scanning electron microscopy image of *C. jejuni*. **C)** Secretome and EVs purification protocol. **D)** Negative staining TEM of purified EVs. **E)** Dynamic light scattering (DLS) measurement of EVs' hydrodynamic diameter in the secretome and after purification. **F)** EVs size distribution measured by nano-flow cytometry **G)** Syto9/Propidium Iodide (PI) assay showing the presence of external (PI) or internal DNA (Syto9) in the vesicles and their respective size. Scale bar: 500 nm.

The presence of internal and external extracellular DNA in EVs suggests different biogenesis of released vesicles. Since small vesicles contained no DNA they were probably the outer membrane vesicles (OMVs) formed by swelling of the outer membrane. In contrast bigger vesicles seem to be outer-inner membrane vesicles (O-IMVs) formed through protrusion of both the outer and cytoplasmic membrane which enables them to carry cytoplasmic DNA.

To detect proteins secreted by *C. jejuni*, a quantitative proteome was performed. The analysis of four independent preparations highlighted the presence of more than 400 secreted cellular proteins (Table S1 of the supplementary data). In terms of molecular functions, most abundant proteins are involved in reaching host cells, adhesion, inflammation, and cell invasion (**Table 1**). The *C. jejuni* Bf used here, is a clinical strain isolated from a French patient in 1994, that is highly virulent but has no gene encoding for cytolethal distending toxins. Despite the absence of toxins, the secretion of proteins involved in host-pathogen interaction in **Table 1**, suggests a cytotoxic potential of purified EVs.

Table 1: The twenty most enriched proteins secreted by *C. jejuni* as determined by proteome analysis.

Protein [a)]	Function / Putative function	Step of the pathogenesis
Che proteins	Chemotaxis proteins	Reaching target cells (chemotaxis)
FlgE	Flagellar hook protein	Reaching target cells (motility), adhesion, invasion
FlgK	Flagellar hook-associated protein	
FlaA, B, C	Flagellins	
GroEL	Molecular chaperone	Adhesion and inflammation
OMP	Fibronectin-binding proteins	Adhesion and inflammation
NLPA proteins	Adhesive lipoproteins	Adhesion
MapA	Outer membrane lipoprotein	Adhesion
HtrA	Serine protease	Invasion
CiaB	*Campylobacter* invasion antigen	Invasion
Peb2	Major antigenic protein	Adhesion, invasion, survival
PorA (MOMP)	Major outer membrane protein	Cell damage (porin) and adhesion

[a)] Raw data of LC-MS/MS analysis of proteins present in *C. jejuni* secretome are available in Table S1 of the supplementary materials.

Cytotoxicity of *C. jejuni* EVs on Caco-2 cells on plates

The MTT viability assay was performed to evaluate the cytotoxic effects of *C. jejuni* EVs and its whole secretome on Caco-2 monolayer in plates. The test was performed in cell culture medium containing 10 % foetal calf serum (FCS) or no serum, to verify whether serum proteins can prevent cytotoxicity of released EVs. After two days of culturing, Caco-2 were incubated with 10% and 20% *C. jejuni* secretome (0.045 mg/mL and 0.1 mg/mL total proteins, respectively) or EVs (MOI of 10) for 24 h. In parallel, cells were incubated with an equivalent volume of PBS as a negative control. In alignment with other *Campylobacter* strains[33,34], the MTT assay showed that *C. jejuni* Bf secretome and EVs significantly affected cells' metabolic activity in culture medium supplemented with 10% FCS, leading to a significant decrease in cell viability compared with the control (**Figure 3A**). However, in serum free medium, the decrease in viability was not statistically relevant compared to the control. This can be explained by the low baseline viability of Caco-2 cells cultivated without FCS (Figure S1). Consequently, the diminished viability of Caco-2 cells likely attenuates the observable cytotoxic effects of the secretome and EVs, indicating the FCS-supplemented medium as the most suitable to study the effects of *C. jejuni* Bf EVs on Caco-2. The cytotoxicity of EVs and secretome was further evaluated using fluorescent microscopy observation of Caco-2 monolayers stained with Hoechst, a nucleus marker, WGA, a membrane marker, and IP, a dead cells nucleus marker (**Figure 3B**). After two days, the epithelialisation process gave rise to a locally confluent monolayer of Caco-2 cells (**Figure 3B**, negative control). However, imaging of cells treated with secretome, EVs or 1 mM H_2O_2 (positive control) indicated that damaged cells detached from the plates. Interestingly, the cytotoxicity of *C. jejuni* EVs at MOI of 10 was similar to that of H_2O_2.

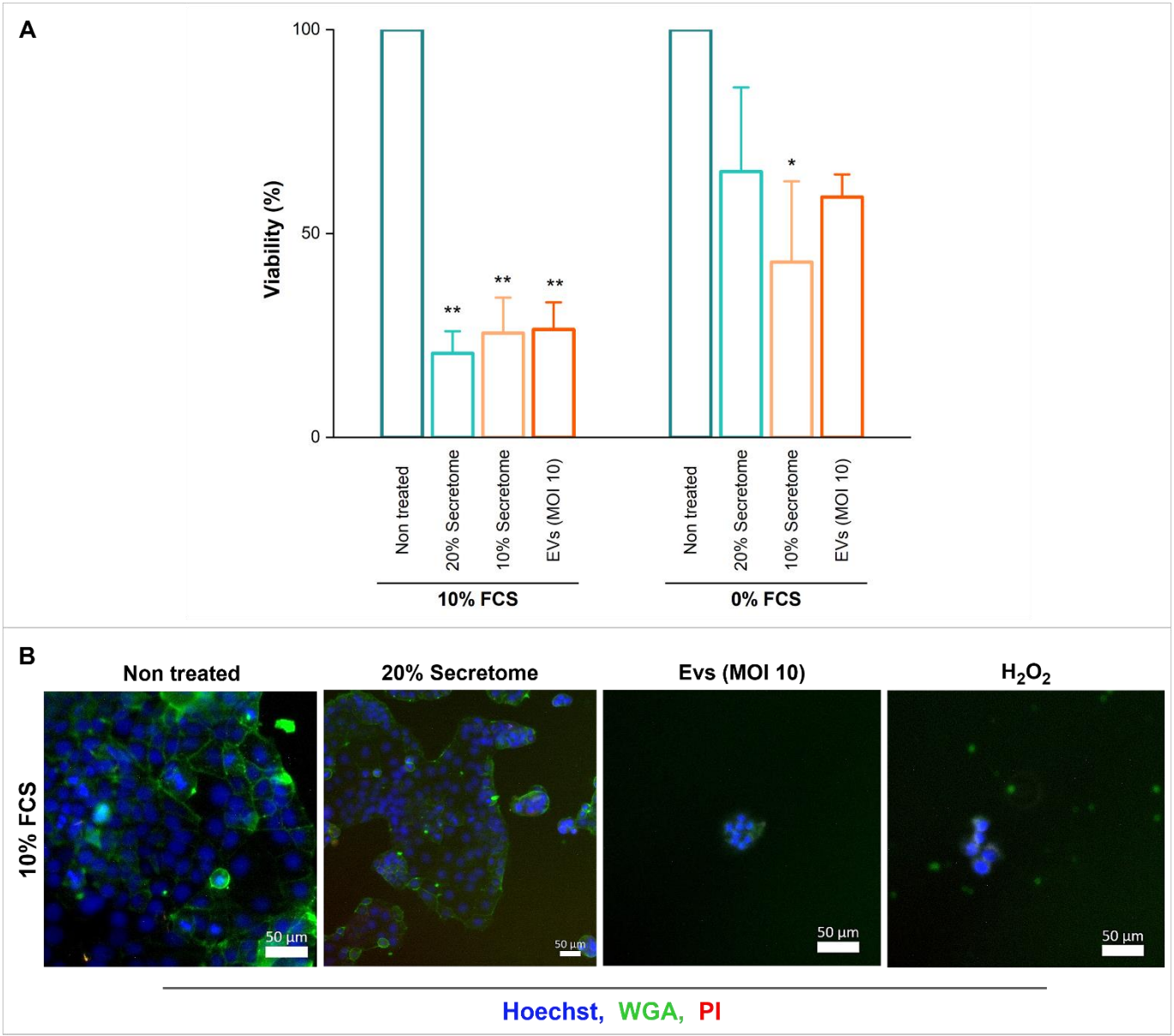

Figure 3: Effect of *C. jejuni* secretome and purified extracellular vesicles (EVs) on Caco-2 cells on plates. A) Cell viability measured via MTT test after incubation for 24 hours with different infections: secretome (20% v/v and 10% v/v), EVs (10% v/v corresponding to $3{\cdot}10^6$ EVs) in DMEM with and without foetal bovine serum. Results are shown as percentage of the negative control (PBS 20 % v/v) ± SD. (Paired comparison t-Test, * p≤0,05 ** p≤0,01 *** p≤0,001, n=3). **B)** Images of the Caco-2 cells on plates after incubation for 24 hours with different infections. Live cells' nuclei labelled with Hoechst blue 3324, dead cells' nuclei with propidium iodide (PI), and membrane protein labelled with WGA. Scale bar: 50 µm.

Engineering a microfluidic chip for epithelial cell culture and real-time analysis

Next, we examined whether the generated Caco-2 monolayer could be cultured within the microfluidic chip. We engineered a device with integrated electrodes using a new simple and rapid fabrication method that provides reliable bonding.

The microfluidic chip consisted of an apical and basal compartment interfaced via a PE tracked-etched membrane, each compartment formed by a PMMA layer carrying gold electrodes and a Flexdym layer with a cut-through channel (**Figure 1**). The electrodes were embedded in the device to eliminate the signal errors that may arise from inconsistent electrode placement during manual insertion and electrode motion. The innovative part of the microfluidic chip was the utilisation of Flexdym as the core polymer of the chip instead of the traditionally employed poly(dimethyl siloxane) (PDMS). Like PDMS, Flexdym is biocompatible, optically transparent, and flexible, but it has lower molecular sorption, and lower gas and water vapour permeability[35]. This makes it more suitable for a gut model since it recreates the hypoxic conditions present in the small intestinal lumen[36]. Furthermore, unlike PDMS,

Flexdym can be hot-embossed and easily bonded enabling a rapid and facile microfabrication process. Finally, due to its reversible bonding characteristic, the separation and reuse of the apical and basal portions of the chip after each experiment was possible, which notably reduced the overall costs and fabrication time.

To validate the device's potential to serve as a gut-on-chip platform for monitoring EV interaction with epithelial cells, we seeded Caco-2 cells on the apical channel to represent the intestinal epithelium. To optimise the coating of the membrane by promoting cell adhesion and differentiation over shorter periods, coatings with poly-L-lysine (0.01%), gelatin (0.1%) and Matrigel (1:3) were tested. Despite all coatings performing well on plate, poly-L-lysine and gelatin performed poorly in the microfluidic system, while good adhesion was obtained with the Matrigel matrix substrate.

We next monitored the growth of Caco-2 cells in the microfluidic device over 48 to 96 hours, using the impedance spectroscopy set-up illustrated in **Figure 4A**. The chip allowed continuous culture for at least 4 days without leakages. The typical impedance spectra for a blank chip and a chip 4 hours after seeding Caco-2 cells are shown in **Figure 4B**, displaying the capability of the device to detect the adhesion of cells to the membrane. **Figure 4C** compares the spectra of Caco-2 cells on day four of culture, before and after incubation with 50 mM hydrogen peroxide for 15 and 60 minutes, showing that the device sensitivity is sufficient to distinguish a vital and damaged epithelium.

The impedimetric measurements were performed over 4 days of Caco-2 culture in the chip under static conditions. **Figure 4D** reports the signals over the entire frequency spectrum of 10 kHz to 100 kHz, while **Figure 4E-G** reports the signals over time at three characteristic frequencies within the measured range (22 kHz, 40 kHz, 99 kHz). For each frequency, the modulus of the impedance ($|Z|$), its real ($Z\ R_e$) and imaginary ($Z\ I_m$) components are plotted. The best distinction between the blank and the cellularised chips was observed in the lower frequency range i.e., ≤ 40 kHz. Signals in this range of frequencies (**Figure 4E** and **4F**) show the lag phase of cell growth during the first 24 h after seeding, followed by an exponential growth phase from 24 h to 72 h, with a maximum impedance increase of 69 kΩ·cm^2 compared to the baseline. The exponential growth was followed by a dying phase, probably due to the limited amount of nutrients caused by the overgrowth. At the highest frequencies tested, the impact of cell growth on the impedance signal is reduced, and only the exponential and dying phases are visible (**Figure 4G**). These results suggest that the real component of the impedance was more sensitive to cell growth compared to its imaginary counterpart. Moreover, the variation in the impedance signal was greatest at 22 kHz, indicating that cell permittivity rises slightly at lower frequencies, as observed previously[37,38].

It is noteworthy that the impedance values observed using our device fall within a similar range (kΩ·cm^2) as those reported in other gut-on-chips[39–41]. However, comparing TEER values within different studies is not straightforward and requires caution. Variations in the TEER values can arise due to temperature variations, number of cell passages, medium composition, electrode materials and position, along with different data readouts and analyses. For these reasons, there is not yet a consensus on the absolute TEER values for Caco-2 cells. Consequently, the electrochemical analysis in complex biological models, like organ-on-chip, provides an approximation rather than a precise indication of the cell status. Although the impedimetric measurements present some limitations, they allow non-invasive and real-time assessments of cell viability and, overall, these results show that the microfluidic chip presented here is suitable for studying intestinal epithelial cell integrity through impedimetric analysis.

Cytotoxicity of *C. jejuni* EVs on Caco-2 cells on chip

Next, we explored the cytotoxicity of *C. jejuni* secretome and EVs on Caco-2 cells grown in the microfluidic chip. For this, the cell suspension was mixed with Matrigel matrix, seeded on the apical channel, and cultured for two days to reach the exponential growth phase. Cells were then incubated with *C. jejuni* secretome (0.1 mg/mL total proteins), or EVs (MOI of 10) in culture medium supplemented with 10 % FCS for 24 h. Incubation with PBS (20 % v/v) and hydrogen peroxide (1mM) were used as negative and positive control, respectively. In addition, since cells in the microfluidic device were grown on a Matrigel substrate, we tested and excluded any protective effect of the Matrigel coating on the infection of Caco-2 with secretome and EVs using MTT assay on 2D culture (Figure S2).

Figure 5 shows the changes in impedance modulus before and after infection with secretome and EVs, along with their respective negative controls.

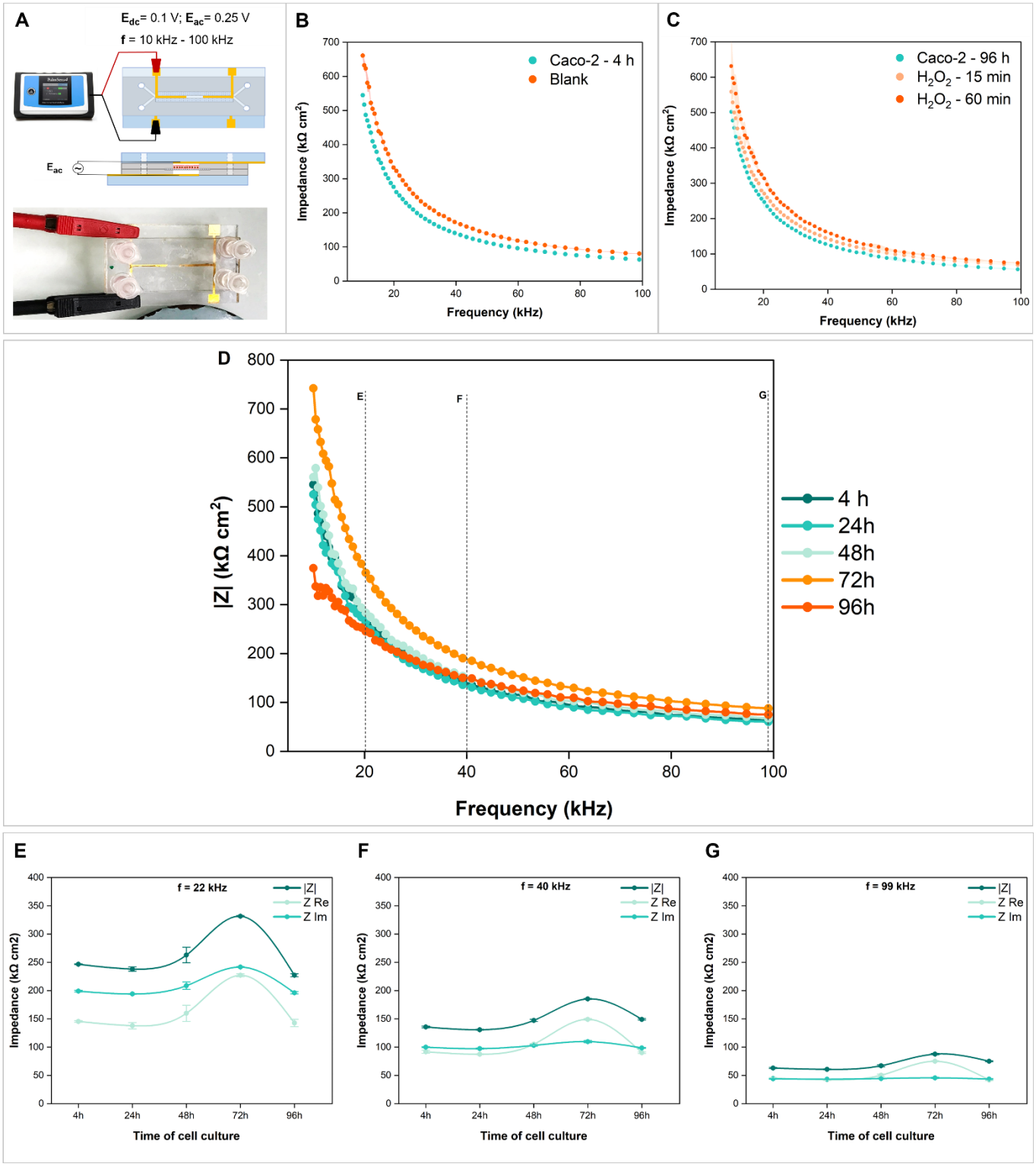

Figure 4: Characterisation of the microfluidic chip. A) Experimental set-up. **B)** Impedance signal recorded without cells (blank) and after Caco-2 adhesion to the membrane, 4 hours after seeding. **C)** Impedance signal recorded at 96 hours of cell culture and after incubation with hydrogen peroxide (H_2O_2) for 15 and 60 minutes**. D)** Impedance magnitude over the entire frequency spectrum(|Z|) and **E-G)** impedance magnitude along with its real (Z Re) and imaginary (Z Im) components measured at three frequencies within the observed frequency range: (E) 22 kHz, (F) 40 kHz, and (G) 99 kHz, throughout a 96-hour cultivation of Caco-2 cells in the chip

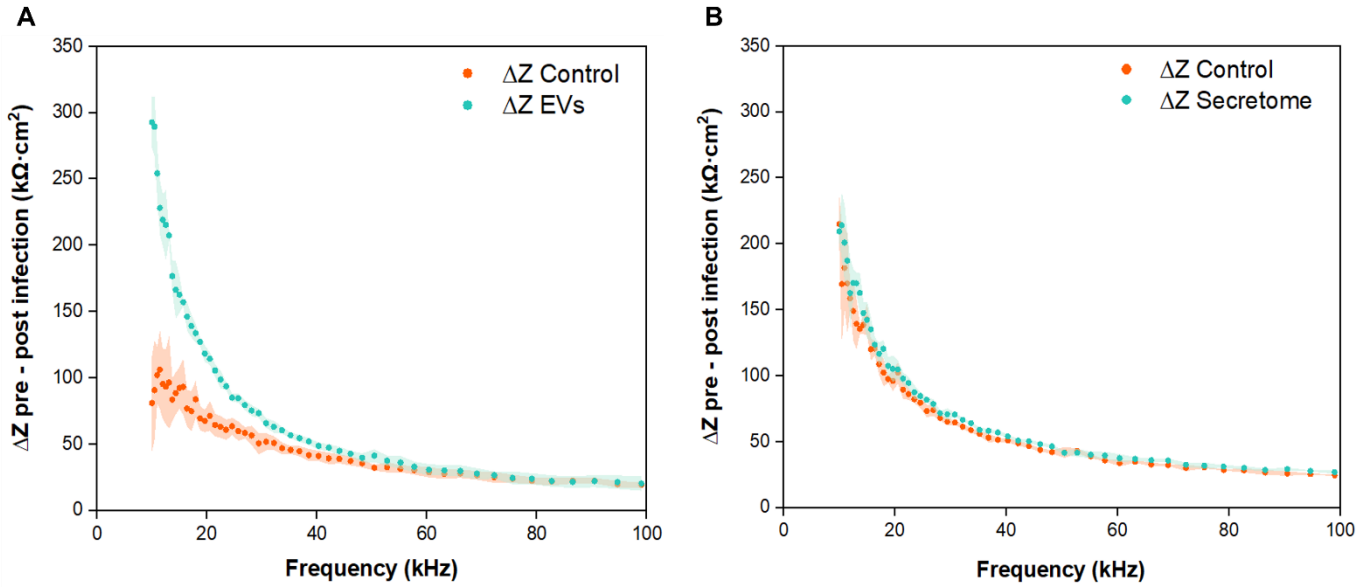

Figure 5: Impedance variation after infection of Caco-2 epithelial cells with *C. jejuni* extracellular vesicles (EVs) and secretome on chip. A) EVs (MOI of 10) and **B)** secretome (20% v/v) were incubated with Caco-2 cells in the microfluidic device for 24 h. The difference between the impedance spectra before and after infection is compared to the respective negative control (PBS 20% v/v). The shaded area represents the SD.

For the cells treated with EVs, the variation in impedance was statistically different from the negative control at the lower frequencies of the spectrum (10–30 kHz); a frequency range previously shown to correlate most strongly with cell behaviour. The greatest difference in impedance variation was observed at 10 kHz, with a delta between pre- and post-infection of 290 kΩ·cm² in the chip treated with EVs, compared to 91 kΩ·cm² in the control (Figure S.3). Conversely, no significant differences were detected between the signals of cells treated with C. jejuni secretome and the negative control. This suggests either that the addition of the C. jejuni secretome altered the matrix composition, thereby interfering with the impedance measurement, or that no cell death occurred, unlike in the cell culture plates. The behaviour of epithelial cells in plates and within the microfluidic device can differ. For instance, discrepancies between in vitro models have been already reported in the context of Caco-2 resistance to cancer treatments, where 3D cellular constructs in a chip exhibited significantly higher resistance to certain chemotherapeutic drugs and irradiation therapy than 2D Caco-2 cultures.[40].

To distinguish between these possibilities, live immunofluorescence imaging was performed to visualise Caco-2 cells within the chip over a culture period of 4 days (**Figure 6**). Four hours after seeding the chips, cell nuclei were stained using Hoechst blue and observed to verify cell adhesion and distribution over the apical microchannel (**Figure 6A-D**). Channel coverage was between 50% and 60% in all the chips seeded, and cell morphology was comparable to that observed in the flask culture. (**Figure 6E-H**, Figure. S.4). After only 24 hours, Caco-2 cells aggregated, forming spheroids with a diameter ranging from 50 to 100 µm, displaying smooth profiles and a morphology consistent with healthy Caco-2 spheroids observed in the literature[42,43] The cells were cultured for 48h and then infected to reproduce the impedance spectroscopy experiments of **Figure 5**. Finally, microscopic observations were performed 24 h post-infection (p.i.) as shown in **Figure 6I-L**.

As expected, cells in the chip treated with PBS were alive and the spheroids maintained their characteristic morphology, while the majority of cells in the chip exposed to hydrogen peroxide died and the spheroids assumed a granular appearance. Remarkably, in agreement with the impedance measurements, no cytotoxic effect of the bacterial secretome on the Caco-2 spheroids grown in the microfluidic platform was observed (**Figure 6K**, and Figure S4). The chip incubated with EVs displayed spheroids with irregular profiles in which the core cells were alive while some of the outermost cells died. This strongly suggests that the spatial 3D organisation of Caco-2 cells obtained in the microfluidic devices protects them from the cytotoxicity of *C. jejuni* secreted biomolecules and EVs.

The observed cytotoxicity of EVs but not of the secretome on peripheral cells of the spheroids suggests that *C. jejuni* virulent factors are mainly transported by EVs. This is expected considering that bacteria of the genus *Campylobacter* do not have a classical secretion system, they rely on the release of membrane vesicles to transport different cargoes, including proteins involved in its interaction with the host.

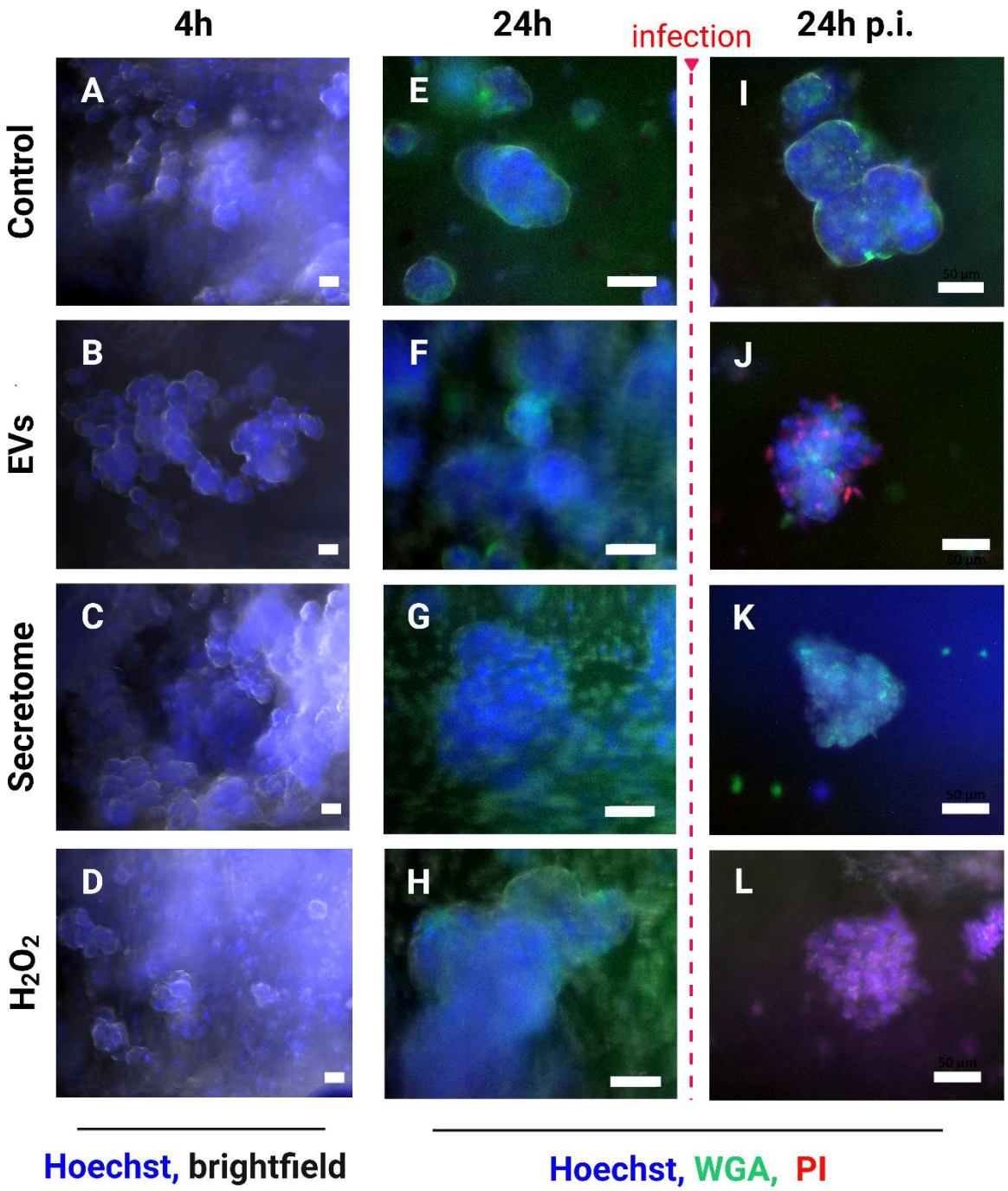

Figure 6: Effect of *C. jejuni* purified extracellular vesicles (EVs) and secretome on Caco-2 cells in the gut-on-chip. Live fluorescence Images of the Caco-2 cells 4h, and 24h after seeding in the gut-on-chip and 24 post infection (p.i.) (corresponding to 72h of culture), with EVs (MOI of 10) and secretome (20% v/v). Cells after infection are compared to the negative control (PBS 20% v/v) and hydrogen peroxide (H_2O_2, 1mM) as positive control. Live cells' nuclei labelled with Hoechst blue 3324, dead cells nuclei with propidium iodide (PI), and membrane protein labelled with WGA. Scale bar: 50 µm.

Conclusions

We reported a new and advanced microfluidic device equipped with built-in electrodes for cultivating and real-time monitoring of intestinal epithelial cell growth and interaction with bacterial virulent factors. We demonstrated that Caco-2 epithelial cells formed spheroids when cultured within the microfluidic chip. Moreover, we identified that Caco-2 spheroids exhibited significantly higher resistance to *C. jejuni* secretome and EVs than Caco-2 organised in 2D monolayer.

Our device possesses several unique features. (*i*) It integrates Flexdym, a polymer which is cost-effective, reusable, and suitable for production in low-resource settings. These characteristics promote wider adoption and accessibility of microfluidic applications, overcoming some of traditional barriers such as long fabrication protocols, costly facilities and single-use prototypes. (*ii*) The Flexdym surface is covered with Matrigel matrix, mimicking the basement membrane necessary for the epithelial cells' adherence and survival. In addition, we show that Matrigel, besides being both cytocompatible and compatible with Flexdym, did not interfere with secretome or EVs. (*iii*) The seeding of human intestinal cell lines results in the formation of spheroids after 24h under static conditions. The chip substrate is covered with densely packed epithelial spheroids providing an *In vitro* model of the intestinal epithelium. (*iv*) The microfluidic platform has imbedded electrodes, allowing real-time on-line measurements with decreased signal noise.

The enhanced resistance of Caco-2 cells self-organised in spheroids to *C. jejuni* vesicles containing various virulence factors highlights the potential of the microfluidic device for studying gastrointestinal bacterial infections and underscores the importance of integrating 3D models into future *In vitro* studies. Beyond infection, the intestine is susceptible to a range of pathologies such as tumours and Crohn's disease. The microfluidic device can be further expanded to incorporate other cell types (i.e., fibroblasts, and mesenchymal stromal cells) and may be a good platform to study host-pathogen interactions, intestinal barrier dysfunctions, exposure to drugs, metabolic stress, diarrheal toxins, or the role of microbiota. Ultimately, all these investigations can be performed with primary cells derived from patients to establish personalised precision medicine.

Author contributions

Experimental work: STC, DP, FR and JMV; Microscopy: DP, ST, CH; Proteomic analysis: CP. Data analysis: STC, JMV; Conceptualisation: JV, ST, GL; Funding acquisition: JV, ER, JBB, MM; writing – original draft: JV, STC; writing – review: JV.

All authors have given approval to the final version of the manuscript.

Conflicts of interest

Authors S.T.C. and J.B.B were employed by the company Eden Tech which sells the Flexdym™. The author E.R. is a co-ownership of Eden Tech. The remaining authors declare no competing financial interest.

Data availability

The data supporting this article have been included as part of the Supplementary Information.

Acknowledgements

We acknowledge and thank Dr Vasa Radonic and Dr Ivana Podunavac for providing the electrode layers of the microfluidic device. We thank the MicrobAdapt team for fruitful discussions and the MIMA2 platform for access to electron microscopy equipment (MIMA2, INRAE, 2018. Microscopy and Imaging Facility for Microbes, Animals and Foods).

This work was supported in part by the IPANEMA project, which received funding from the European Union's Horizon 2020 research and innovation program under grant agreement No 872662, and the French National Agency for Research (ANR-21-CE21-009 SIENA and ANR-21-CE42 ELISE projects, to J.V.).

STC has received funding from SmartAge project, the European Union's Horizon 2020 research and innovation program under the Marie Skłodowska-Curie grant agreement No 859890.

Notes and references

1 K. E. Rudd, S. C. Johnson and K. M. Agesa, *The Lancet*, 2022, **400**, 2221–2248.
2 World Health Organization (WHO)., *Campylobacter Fact Sheet*, 2020.
3 *EFSA Journal*, , DOI:10.2903/j.efsa.2023.7867.
4 R. E. Black, M. M. Levine, M. Lou Clements, T. P. Hughes and M. J. Blaser, *Experimental Campylobacter jejuni Infection in Humans*, 1988, vol. 157.
5 V. Kreling, F. H. Falcone, C. Kehrenberg and A. Hensel, *Appl Microbiol Biotechnol*, 2020, **104**, 10409–10463.
6 S. Mousavi, S. Bereswill and M. M. Heimesaat, *Microorganisms*, 2020, 8.
7 J. Malet-Villemagne and J. Vidic, *ChemRxiv*, , DOI:10.26434/chemrxiv-2024-8b9sz.
8 C. Y. M. Luk, S. A. Lee, N. Naidovski, F. Liu, A. C. Y. Tay, L. Wang, S. Riordan and L. Zhang, *Front Microbiol*, 2024, **14**, 1–12.
9 A. J. Maccallum, D. Harris, G. Haddock and P. H. Everest, *Microbiology (N Y)*, 2006, **152**, 3661–3665.
10 S. M. Callahan, C. G. Dolislager and J. G. Johnson, *Infect Immun*, 2021, **89**, 116–21.
11 D. R. Buelow, J. E. Christensen, J. M. Neal-mckinney and M. E. Konkel, *Mol Microbiol*, 2011, **80**, 1296–1312.
12 S. Hatayama, T. Shimohata, S. Amano, J. Kido and A. Q. Nguyen, *Front Cell Infect Microbiol*, 2018, **8**, 1–12.
13 I. Sharafutdinov, N. Tegtmeyer, M. Rohde, A. Olofsson, Z. Rehman, A. Arnqvist and S. Backert, *Cells*.
14 L. H. M. Le, B. Elgamoudi, N. Colon, A. Cramond, F. Poly, L. Ying, V. Korolik and R. L. Ferrero, *Microbiol Spectr*, , DOI:10.1128/spectrum.03232-23.
15 A. Elmi, F. Nasher, H. Jagatia, O. Gundogdu, M. Bajaj-elliott, B. Wren and N. Dorrell, 2016, **18**, 561–572.
16 B. Zalewska-Piatek, M. Olszewski, T. Lipniacki, S. Błonski, S. Nowicki and R. Piatek, *PLoS Pathog*, 2020, **16**, 1–32.

17 A. Park, H. Jeong, J. Lee, K. P. Kim and C. Lee, *Biochip J*, 2011, **5**, 236–241.
18 M. Lemos, F. Mergulhão, L. Melo and M. Simões, *Food and Bioproducts Processing*, 2014, 1–7.
19 E. Sherman, K. Bayles, D. Moormeier and J. Endres, *mSphere*, 2019, **4**, e00372-19.
20 S. T. Calzuola, G. Newman, T. Feaugas, C. M. Perrault, J.-B. Blondé, E. Roy, C. Porrini, M. Stojanovic and J. Vidic, , DOI:10.26434/chemrxiv-2024-snl73.
21 A. Grassart, V. Malardé, S. Gobba, A. Sartori-Rupp, J. Kerns, K. Karalis, B. Marteyn, P. Sansonetti and N. Sauvonnet, *Cell Host Microbe*, 2019, **26**, 435-444.e4.
22 A. Boquet-pujadas, T. Feaugas, A. Petracchini, A. Grassart, H. Mary, M. Manich, S. Gobaa, N. Sauvonnet and E. Labruyère, *Sci Adv*, 2022, 1–18.
23 H. J. Kim, D. Huh, G. Hamilton and D. E. Ingber, *Lab Chip*, 2012, **12**, 2165–2174.
24 U. C. Ghoshal and U. Ghoshal, *Gastroenterology Clinics of NA*, 2017, **46**, 103–120.
25 V. Bronnec, H. Turoňová, A. Bouju, S. Cruveiller, R. Rodrigues, K. Demnerova, O. Tresse, N. Haddad and M. Zagorec, *Front Microbiol*, , DOI:10.3389/fmicb.2016.01002.
26 S. Auger, C. Henry, C. Péchoux, S. Suman, N. Lejal, N. Bertho, T. Larcher, S. Stankic and J. Vidic, *Sci Rep*, , DOI:10.1038/s41598-018-30719-9.
27 J. Vidic, C. A. Richard, C. Péchoux, B. Da Costa, N. Bertho, S. Mazerat, B. Delmas and C. Chevalier, *Journal of Biological Chemistry*, 2016, **291**, 739–751.
28 I. Moser, W. Schroeder and J. Salnikow, *FEMS Microbiol Lett*, 2006, **157**, 233–238.
29 C. M. Thomas and K. M. Nielsen, *Nat Rev Microbiol*, 2005, **3**, 711–721.
30 J. Feng, L. Ma, J. Nie, M. E. Konkel and X. Lu, *Appl Environ Microbiol*, , DOI:10.1128/AEM.02068-17.
31 H. Hemmi, O. Takeuchi, T. Kawai, T. Kaisho, S. Sato, H. Sanjo, M. Matsumoto, K. Hoshino, H. Wagner, K. Takeda and S. Akira, *Nature*, 2000, **408**, 740–745.
32 D. Islam, L. Bandholtz, J. Nilsson, H. Wigzell, B. Christensson, B. Agerberth and G. H. Gudmundsson, *Nat Med*, 2001, **7**, 180–185.
33 M. Montanari, M. Guescini, O. Gundogdu, F. Luchetti, P. Lanuti, C. Ciacci, S. Burattini, R. Campana, C. Ortolani, S. Papa and B. Canonico, *Int J Mol Sci*, , DOI:10.3390/ijms24010487.
34 H. M. L. Le, B. Elgamoudi, N. Colon, A. Cramond, F. Poly, L. Ying, V. Korolik and R. L. Ferrero, *Microbioloy Spectrum*, 2024, 1–17.
35 H. Nguyen, H. Thach, E. Roy, K. Huynh and C. M. Perrault, *Micromachines (Basel)*, , DOI:10.3390/mi9090461.
36 L. Zheng, C. J. Kelly and S. P. Colgan, *Am J Physiol Cell Physiol*, 2015, **309**, 350–360.
37 N. Nasir and M. Al Ahmad, *Journal of Egineering*.
38 I. Podunavac, T. Kneži, M. Djisalov, N. Omerovic, M. Radovic, L. Janjuševi, D. Stefanovic, M. Panic, I. Gadjanski and V. Radonic, *Sensors*.
39 A. Pierron, S. Mimoun, L. S. Murate, N. Loiseau and Y. Lippi, *Arch Toxicol*, 2016, **90**, 2037–2046.
40 T. Miyazaki, J. Yang, S. Imamura, Y. Hirai, K. Kamei, T. Tsuchiya and O. Tabata, in *IEEE Micro Electro Mechanical Systems (MEMS)*, 2021, pp. 411–414.
41 L. Wang, J. Han, W. Su, A. Li, W. Zhang, H. Li, H. Hu, W. Song, C. Xu and J. Chen, *Microsyst Nanoeng*, , DOI:10.1038/s41378-022-00447-2.
42 E. Gheytanchi, M. Naseri, F. Karimi-Busheri, F. Atyabi, E. S. Mirsharif, M. Bozorgmehr, R. Ghods and Z. Madjd, *Cancer Cell Int*, 2021, **21**, 1–16.
43 J. Koch, D. Monch, A. Maaß, C. Gromoll, T. Hehr, T. Leibold, H. J. Schlitt, M.-H. Dahlke and P. Renner, *PLoS One*, 2021, **16**, 1–13.